Comput Mech (2014) 53:309–324
DOI 10.1007/s00466-013-0909-9

ORIGINAL PAPER

A weighted collocation on the strong form with mixed radial basis approximations for incompressible linear elasticity

Sheng-Wei Chi · Jiun-Shyan Chen · Hsin-Yun Hu

Received: 26 June 2013 / Accepted: 31 July 2013 / Published online: 17 August 2013

Abstract A weighted strong form collocation framework with mixed radial basis approximations for the pressure and displacement fields is proposed for incompressible and nearly incompressible linear elasticity. It is shown that with the proper choice of independent source points and collocation points for the radial basis approximations in the pressure and displacement fields, together with the analytically derived weights associated with the incompressibility constraint and boundary condition collocation equations, optimal convergence can be achieved. The optimal weights associated with the collocation equations are derived based on achieving balanced errors resulting from domain, boundaries, and constraint equations. Since in the proposed method the overdetermined system of the collocation equations is solved by a least squares method, independent pressure and displacement approximations can be selected without suffering from instability due to violation of the LBB stability condition. The numerical solutions verify that the solution of the proposed method does not exhibit volumetric locking and pressure oscillation, and that the solution converges exponentially in both L_2 norm and H_1 semi-norm, consistent with the error analysis results presented in this paper.

S.-W. Chi (✉)
Civil and Materials Engineering Department ,
University of Illinois, Chicago, IL, USA
e-mail: swchi@uic.edu

J.-S. Chen
Civil and Environmental Engineering Department,
University of California, Los Angeles, CA, USA

H.-Y. Hu
Applied Mathematics Department, Tunghai University,
Taichung, Taiwan, ROC

1 Introduction

The recent development of meshfree and particle methods [1–5] expands a new horizon to computational mechanics. These methods for solving partial differential equations do not rely on the mesh connectivity for construction of the approximation functions. The approximation functions used in meshfree methods can be classified into two families. One family of approximation functions equips with the polynomial reproductivity properties, for example, the moving least squares (MLS) [1] and reproducing kernel (RK) [2,6] approximation functions. These functions are compactly supported and are generally rational functions. The other family of meshfree approximation functions, on the other hand, does not enforce polynomial reproductivity in their construction, for example, the nonlocal radial basis functions (RBFs) [7,8]. Element Free Galerkin (EFG) [1] method and Reproducing Kernel Particle Method (RKPM) [2,6] introduce MLS and RK functions, respectively, into the Galerkin weak formulation. Alternatively, the reproducing kernel collocation method (RKCM) employs compactly supported RK approximation directly in the strong form sampling at the collocation points [9,10], whereas the radial basis collocation method (RBCM) introduces the nonlocal RBFs in the strong form collocation. In general, the numerical methods for solving PDEs based on weak formulation with compactly supported approximation functions are more stable, however, with convergence properties affected by both the employed approximation functions and the quadrature rules used in the domain integration. In contrast, the numerical methods based on a direct discretization of strong form at collocation points, such as RBCM and RKCM exhibit convergence behavior largely influenced by the employed approximation functions without the restriction of meeting certain requirements in the quadrature rules. Comprehensive investigation

has shown that RKCM with RK approximation offers an algebraic convergence [9,10], while RBCM with RBF approximation exhibits an exponential convergence [8,11,12].

Kansa [7,8] first introduced the multiquadrics RBF for solving PDEs and initiated a widespread research and application related to RBCM. Franke and Schaback [13] and Hu et al. [14] studied the theoretical aspects of solving PDEs with collocation based on RBF approximation. Wendland [15] derived error estimates of combining the RBF and the Galerkin method for solving PDEs, and this combined approach leads to the same error properties in the energy norm as that in the classical finite element method. Hu et al. [11] showed that the RBCM solution can be optimized if boundary conditions are properly weighted. Cecil et al. [16] provided a numerical scheme based on the RBF for Hamilton-Jacobi equations using an unstructured discretization in arbitrary dimensions. Pollandt [17] used RBFs as the approximation in a multidimensional boundary element method to solve nonlinear elliptic PDEs. Sonar [18] used RBFs for local reconstruction of solutions in solving hyperbolic conservation law, and showed that the thin-plate RBF helps to improve the accuracy of the finite volume methods for the hyperbolic equations. Chi et al. [19] demonstrated a significantly small dispersion error in RBCM compared to that in the FEM for the same level of discretization. Chen et al. introduced a subdomain collocation method for heterogeneous elasticity [12] and fracture mechanics [20]. Much effort has been also devoted to the localization of RBFs to yield a sparse system with better conditioning. Wendland [21] introduced a class of positive definite and compactly supported radial basis functions (CSRBF) which consist of a univariate polynomial within their support. The accuracy of the approach can be improved by using a large scaling factor but is costly. Chen et al. [22] proposed a reproducing kernel enhanced RBF approximation to achieve a local approximation, which holds the similar convergence property as that of the RBF collocation method while yielding a banded and better-conditioned discrete system.

Despite great efforts for decades, incompressible problems remain challenging in computational mechanics. Without proper numerical techniques, the numerical solutions suffer from either locking or instability in the incompressible limit. Hermann [23] was the first to identify the fundamental difficulties associated with displacement based finite element formulation. Many mixed formulations have been introduced to resolve the locking. The $u - p$ mixed formulation by Herrmann [23] was the first effective method for solving incompressible elasticity, and it can be considered as a reduced form of the Hellinger-Reissner variational principle. Murakawsa and Atlur [24] introduced hybrid stress formulations for nonlinear incompressible materials. Pian and Sumihara [25] introduced two-field elements based on interpolation of stress and displacement fields, and later Simo and Rifai [26] proposed an enhanced strain formulation based on the three-field Hu-Washizu variational theorem. Although the above mentioned mixed elements by Pian et al. and by Simo et al. remove the incompressible locking, they are typically sensitive to mesh distortion due to the transformation in stress or strain fields. Mixed formulation has also been extended by Liu et al. [27] using Hu-Washizu theorem for bending and incompressible hyperelasticity and Chen et al. [28] by a volumetric strain projection method for nonlinear incompressible problems. The mixed formulation, however, yields a saddle point problem which could lead to instability under improper combination of approximation functions for different field variables. The celebrated Babuška-Brezzi or LBB stability condition [29,30] provides the mathematical foundation of mixed methods though its verification is not an easy task. Many attempts have been made to stabilize the numerical solutions, such as those based the perturbed Lagrangian and augmented Lagrangian formulations in the displacement-pressure mixed formulation (Sani et al. [31]; Sussman and Bathe [32]; Hughes [33]; Chen et al. [34]) and the pressure projection method (Chen et al. [35,36]).

On the other hand, many finite element formulations have also been proposed using the displacement as the only unknown. The concept of reduced integration by Fried [37] and Zienkiewicz et al. [38] for constrained problems has been extended to the selective reduced integration by Malkus and Hughes [39] in which the unknowns for pressure and enhanced strain are condensed locally, and it was later generalized as a B-bar method by Hughes [40]. Other effective displacement-based methods are hourglass control on under integrated elements by Belytschko et al. [41], and explicit incompressible plane strain element using the Taylor series expansion by Liu et al. [42]. Some researchers considered embedding the divergence free condition in the displacement approximation. Vidal et al. [43] imposed the pseudo-divergence free approximate within the MLS shape function to partially alleviate the volumetric locking. Lovadina et al. [44] reformulated the incompressible elastic problem as an elliptic fourth order problem in terms of a stream function whose *curl* gives the displacement solution. The stream function is constructed based on the non-uniform rational B-splines (NURBS) [45] in order to fulfill the required regularity, and the incompressibility constraint is exactly satisfied. The divergence free condition has also been introduced into the meshfree enhanced finite element formulation by Wu et al. [46].

The convexity of least-squares methods for numerical solution of PDEs naturally avoids the stability issue (violation of inf-sup condition) in the Galerkin type mixed formulation, and hence, as long as the locking is avoided, the formulation can be straightforward. Franca and Stenberg [47] proposed a mixed finite element method in an augmented Galerkin formulation with least-squares terms, in which the

augmented stress, pressure, and displacement are separately approximated. Cai et al [48] proposed a two-stage least-squares finite element approach in which the displacement gradient is first solved and followed by the solution of displacement field. The drawback of using finite element in the least-squares method is that the second order problem needs to be broken down into a system of first order problems due to the regularity limitation of finite elements. In this work, we introduce a mixed formulation with smooth approximations for incompressible problem based on the collocation of the strong form. The pressure and displacement fields are independent variables approximated by RBFs. Since the strong form collocation method can be related to the discretization of a least-squares functional, the selection of pressure and displacement approximations is not restricted to the LBB stability condition in the proposed approach. In this approach, the key to achieve optimal convergence is to properly weight the collocation equations of the PDE, Neumann and Dirichlet boundary conditions, and incompressibility constraint. Error analysis will be performed in this work to obtain those weights based on error balancing between the four sets of collocation equations.

This paper is organized as follows. Section 2 demonstrates the numerical difficulties in the displacement based RBCM for incompressible elasticity. We show that the displacement based RBCM exhibits volumetric locking in the incompressible limit through the eigenvalues in the modal analysis and an elasticity benchmark problem. The pressure-displacement mixed formulation in conjunction with the strong form collocation method is introduced in Sect. 3. The proper weights to balance the errors between domain, boundary, and incompressible constraint collocation equations for optimal convergence are also derived. Several numerical examples are given in Sect. 4 to demonstrate the performance of the proposed method in the incompressible problem. Conclusions and remarks are given in Sect. 5.

2 Difficulty of RBCM in the limit of incompressibility

In this Section we examine the numerical performance of radial basis collocation method for linear elasticity in the limit of incompressibility. For this purpose, consider the following boundary value problem:

$$\sigma_{ij,j} + b_i = 0 \quad \text{in} \quad \Omega \tag{1}$$

$$\sigma_{ij} n_j = h_i \quad \text{on} \quad \partial\Omega^h \tag{2}$$

$$u_i = g_i \quad \text{on} \quad \partial\Omega^g \tag{3}$$

with the homogenous isotropic constitutive law

$$\sigma_{ij} = \lambda \varepsilon_{kk} \delta_{ij} + 2\mu \varepsilon_{ij} \tag{4}$$

where σ_{ij} is the Cauchy stress tensor; $\varepsilon_{ij} = u_{(i,j)} = \frac{1}{2}(u_{i,j} + u_{j,i})$ is the strain tensor; $(\cdot)_{,j} \equiv \partial(\cdot)/\partial x_j$; λ and μ are Lamé constants; b_i is the body force; u_i is the displacement; Ω is the open domain with a closed boundary $\partial\Omega$; $\partial\Omega^h$ and $\partial\Omega^g$ are the Neumann and Dirichlet boundaries, respectively; $\partial\Omega = \partial\Omega^h \cup \partial\Omega^g$; h_i is the surface traction on $\partial\Omega^h$; n_i is the surface outward normal on $\partial\Omega^h$; g_i is the prescribed displacement on $\partial\Omega^g$.

A set of RBFs, $\{g_I(\mathbf{x})\}_{I=1}^{Ns}$, is constructed entirely based on a set of Ns points, called the source points, in a closed domain, $\mathbf{S} = [\mathbf{x}_1, \mathbf{x}_2, \cdots \mathbf{x}_{N_s}] \subseteq \hat{\Omega}$. Although not a necessity, $\hat{\Omega}$ is often chosen to be identical to the problem domain, $\Omega \cup \partial\Omega$. It has been shown that $g_I(\mathbf{x})$ are linearly independent if the source points are distinct [49]. Thus, the displacement u_i can be approximated by the linear combination of RBFs as

$$u_i \approx u_i^h = \sum_{I=1}^{Ns} g_I d_{iI} \tag{5}$$

or in a matrix form:

$$\mathbf{u}^h = \mathbf{G}\mathbf{d} \tag{6}$$

where $\mathbf{G} = \left[\mathbf{g}_1, \mathbf{g}_2, \ldots, \mathbf{g}_{Ns}\right]$, $\mathbf{g}_I = g_I \mathbf{I}$, $\mathbf{d} = [\mathbf{d}_1, \mathbf{d}_2, \ldots, \mathbf{d}_{Ns}]^T$, and $\mathbf{d}_I = [d_{1I}, d_{2I}, d_{3I}]^T$.

As RBFs are continuous functions, the derivatives of the approximation can be obtained in a straightforward manner by $D^\alpha u_i^h(\mathbf{x}) = \sum_{I=1}^{Ns} D^\alpha g_I(\mathbf{x}) d_{iI}$, where $D^\alpha u_i \equiv \partial^{|\alpha|} u_i / \partial x_1^{\alpha_1} \cdots \partial x_d^{\alpha_d}$, $|\alpha| = \sum_{i=1}^{d} \alpha_i$, is the differential operator. Commonly used RBFs, multiquadric (MQ) and Gaussian RBFs are given as follows:

$$g_I(\mathbf{x}) = (r_I^2 + a^2)^{n-\frac{3}{2}}, \quad n = 1, 2, \ldots \text{ (MQ RBF)} \tag{7}$$

$$g_I(\mathbf{x}) = \exp\left(-\frac{r_I^2}{a^2}\right) \text{ (Gaussian RBF)} \tag{8}$$

where $r_I = \|\mathbf{x} - \mathbf{x}_I\|$ and a is a constant, called the shape parameter. For MQ RBF, when $n = 1$, the function is called the inverse MQ (IMQ). Unless otherwise stated, the IMQ is adopted in this study.

In the RBCM, the approximation in Eq. (5) is introduced into Eqs. (1)–(3), and the residuals are enforced to be zero at a set of collocation points $\{\xi_J\}_{J=1}^{Nc} \in \Omega \cup \partial\Omega$, to yield:

$$\begin{aligned} &\boldsymbol{\mathcal{L}}(\mathbf{G}(\xi_J))\mathbf{d} = \mathbf{f}(\xi_J) && \forall \xi_J \in \Omega \\ &\boldsymbol{\mathcal{B}}^h(\mathbf{G}(\xi_J))\mathbf{d} = \mathbf{h}(\xi_J) && \forall \xi_J \in \partial\Omega^h \\ &\boldsymbol{\mathcal{B}}^g(\mathbf{G}(\xi_J))\mathbf{d} = \mathbf{g}(\xi_J) && \forall \xi_J \in \partial\Omega^g \end{aligned} \tag{9}$$

In the two dimensional elasticity as an example, the operator matrices $\boldsymbol{\mathcal{L}}$, $\boldsymbol{\mathcal{B}}^h$, and $\boldsymbol{\mathcal{B}}^g$ are

$$\boldsymbol{\mathcal{L}} = \begin{bmatrix} (\lambda+2\mu)\frac{\partial^2}{\partial x_1^2} + \mu\frac{\partial^2}{\partial x_2^2} & (\lambda+\mu)\frac{\partial^2}{\partial x_1 \partial x_2} \\ (\lambda+\mu)\frac{\partial^2}{\partial x_1 \partial x_2} & (\lambda+2\mu)\frac{\partial^2}{\partial x_2^2} + \mu\frac{\partial^2}{\partial x_1^2} \end{bmatrix} \tag{10}$$

$$\mathcal{B}^h = \begin{bmatrix} (\lambda+2\mu)n_1\frac{\partial}{\partial x_1}+\mu n_2\frac{\partial}{\partial x_2} & \lambda n_1\frac{\partial}{\partial x_2}+\mu n_2\frac{\partial}{\partial x_1} \\ \lambda n_2\frac{\partial}{\partial x_1}+\mu n_1\frac{\partial}{\partial x_2} & (\lambda+2\mu)n_2\frac{\partial}{\partial x_2}+\mu n_1\frac{\partial}{\partial x_1} \end{bmatrix} \tag{11}$$

$$\mathcal{B}^g = \begin{bmatrix} 1 & 0 \\ 0 & 1 \end{bmatrix} \tag{12}$$

The above equation for boundary value problem in Eqs. (1)–(3) has the following exponential convergence property:

$$\left\| \mathbf{u} - \mathbf{u}^h \right\|_\ell \leq C_\nu \eta^{a/H} \left\| \mathbf{u} \right\|_t \tag{13}$$

where $0 < \eta < 1$, H is the radial distance $H := H(\Omega, \mathbf{S}) = \sup_{x\in\Omega} \min_{x_I\in\mathbf{S}} \|x - x_I\|$, C_ν is a generic constant with the subscript ν denoting that it is dependent on the Poisson's ratio ν, $\|\cdot\|_\ell$ is the Sobolev ℓ-norm, and $\|\cdot\|_t$ is induced from the regularity requirements of the approximated function $\boldsymbol{u}$ and RBFs, see [50,51].

Equation 9 can be recast into a matrix form as:

$$\mathbf{Kd} = \mathbf{f} \tag{14}$$

Note that when $Nc > Ns$, Eq. (14) leads to an overdetermined system, and a least-squares method can be applied for the solution by minimizing a weighted residual. The residual can be defined as $e(\mathbf{d}) = \frac{1}{2}(\mathbf{Kd} - \mathbf{f})^T\mathbf{W}(\mathbf{Kd} - \mathbf{f})$, where $\mathbf{W}$ a symmetric weighting matrix, Minimizing $e(\mathbf{d})$ yields

$$\mathbf{K}^T\mathbf{WKd} = \mathbf{K}^T\mathbf{Wf} \tag{15}$$

It has been shown [11] that solving strong form collocation by a least-squares method is equivalent to minimizing a least-squares functional with quadrature. The problem statement can be rephrased as: find $\mathbf{u}^h$ such that

$$E(\mathbf{u}^h) = \inf_{v\in V} E(\mathbf{v}) \tag{16}$$

where V is the finite dimensional space spanned by RBFs, and

$$\begin{aligned} E(\mathbf{v}) = \tfrac{1}{2}\hat{\int_\Omega}(\mathcal{L}\mathbf{v} - \mathbf{f})^2 d\Omega + \tfrac{1}{2}\hat{\int_{\partial\Omega^h}}(\mathcal{B}^h\mathbf{v} - \mathbf{h})^2 d\Gamma \\ + \tfrac{1}{2}\hat{\int_{\partial\Omega^g}}(\mathcal{B}^g\mathbf{v} - \mathbf{g})^2 d\Gamma \end{aligned} \tag{17}$$

Here $\hat{\int}$ denotes the integration with quadrature. In Chen et al. [11], an error estimate has been provided as follows:

$$\begin{aligned} \|\mathbf{u} - \mathbf{u}_{Ns}\|_A \leq C_1\kappa \|\mathbf{u} - \mathbf{v}\|_{2,\Omega} + C_2\kappa \|\partial(\mathbf{u} - \mathbf{v})/\partial n\|_{0,\partial\Omega^h} \\ + C_3 \|\mathbf{u} - \mathbf{v}\|_{0,\partial\Omega^g} \end{aligned} \tag{18}$$

with a norm defined as

$$\|\mathbf{v}\|_A = \left(\|\mathcal{L}\mathbf{v}\|^2_{0,\Omega} + \|\mathbf{v}\|^2_{1,\Omega} + \left\|\mathcal{B}^h\mathbf{v}\right\|^2_{0,\partial\Omega^h} + \left\|\mathcal{B}^g\mathbf{v}\right\|^2_{0,\partial\Omega^g} \right)^{1/2} \tag{19}$$

It is evident from Eq. (18) that the errors in Eq. (17) are unbalanced, with a factor of material constant $\kappa = 2\mu + 3\lambda$, between terms associated with the domain Ω and boundaries $\partial\Omega^h$ and $\partial\Omega^g$. Therefore, a weighted collocation method has been introduced to obtain an optimal solution accurate and convergent. To formulate the weighted collocation equation, consider its least-squares functional counterpart:

$$\begin{aligned} E(\mathbf{v}) = \tfrac{1}{2}\hat{\int_\Omega}(\mathcal{L}\mathbf{v} - \mathbf{f})^2 d\Omega + \tfrac{\alpha^h}{2}\hat{\int_{\partial\Omega^h}}(\mathcal{B}^h\mathbf{v} - \mathbf{h})^2 d\Gamma \\ + \tfrac{\alpha^g}{2}\hat{\int_{\partial\Omega^g}}(\mathcal{B}^g\mathbf{v} - \mathbf{g})^2 d\Gamma \end{aligned} \tag{20}$$

Define a norm as

$$\begin{aligned} \|\mathbf{v}\|_B = (\|\mathcal{L}\mathbf{v}\|^2_{0,\Omega} + \|\mathbf{v}\|^2_{1,\Omega} + \alpha^h \left\|\mathcal{B}^h\mathbf{v}\right\|^2_{0,\partial\Omega^h} \\ + \alpha^g \left\|\mathcal{B}^g\mathbf{v}\right\|^2_{0,\partial\Omega^g})^{1/2} \end{aligned} \tag{21}$$

Correspondingly, we have the following error estimate [11]:

$$\begin{aligned} \|\mathbf{u} - \mathbf{u}_{Ns}\|_B &\leq C_4\kappa \|\mathbf{u} - \mathbf{v}\|_{2,\Omega} + C_5\kappa\sqrt{\alpha^h} \|\partial(\mathbf{u} - \mathbf{v})/\partial n\|_{0,\partial\Omega^h} \\ &\quad + C_6\sqrt{\alpha^g} \|\mathbf{u} - \mathbf{v}\|_{0,\partial\Omega^g} \\ &\leq C_7\kappa Ns \|\mathbf{u} - \mathbf{v}\|_{1,\Omega} + C_8\kappa Ns\sqrt{\alpha^h} \|\mathbf{u} - \mathbf{v}\|_{1,\Omega} \\ &\quad + C_9\sqrt{\alpha^g} \|\mathbf{u} - \mathbf{v}\|_{1,\Omega} \end{aligned} \tag{22}$$

To balance the errors associated with each term in (22), the weights have been selected as $\sqrt{\alpha^h} \approx O(1)$ and $\sqrt{\alpha^g} \approx O(\kappa N_s)$. It has also been shown numerically that $\kappa = \max(\lambda, \mu)$ gives the optimal accuracy [11] when the Poisson's ratio ν is not close to 0.5. However, when ν approaches 0.5, $\lambda = \frac{2\mu\nu}{1-2\nu}$ grows unboundedly, and hence κ. As a result, it leads to an ill-conditioned discrete system with solution deterioration. A better weight can be selected by considering the Korn's inequality [52] for incompressibility limit. It has been shown that if certain regularity is satisfied [52], the following estimate holds for a generic constant C which is independent of λ.

$$\|\mathbf{v}\|_2 + \frac{\lambda}{\mu}\|\nabla\cdot\mathbf{v}\|_1 \leq C\|\mathbf{f}\| \tag{23}$$

This estimate suggests that the divergence of the displacement has a different scale from displacement itself with a factor of $\frac{\lambda}{\mu}$ [47]. Therefore, for problems with the Poisson's ratio close to 0.5, the weight $\sqrt{\alpha^g} \approx O(\mu Ns)$ should be selected.

Minimizing Eq. (20) is equivalent to solving the following weighted collocation equations by a least squares method.

$$\begin{aligned}
&\mathcal{L}\left(\mathbf{G}(\xi_J)\right)\mathbf{d} = \mathbf{f}(\xi_J) && \forall \xi_J \in \Omega \\
&\sqrt{\alpha^h}\mathcal{B}^h\left(\mathbf{G}(\xi_J)\right)\mathbf{d} = \sqrt{\alpha^h}\mathbf{h}(\xi_J) && \forall \xi_J \in \partial\Omega^h \\
&\sqrt{\alpha^g}\mathcal{B}^g\left(\mathbf{G}(\xi_J)\right)\mathbf{d} = \sqrt{\alpha^g}\mathbf{g}(\xi_J) && \forall \xi_J \in \partial\Omega^g
\end{aligned} \tag{24}$$

In the matrix form it can expressed as

$$\begin{bmatrix} \mathbf{L} \\ \sqrt{\alpha^h}\mathbf{B}^h \\ \sqrt{\alpha^g}\mathbf{B}^g \end{bmatrix} \mathbf{d} = \begin{bmatrix} \mathbf{f} \\ \sqrt{\alpha^h}\mathbf{h} \\ \sqrt{\alpha^g}\mathbf{g} \end{bmatrix} \tag{25}$$

The solution of Eq. (25) can be obtained by minimizing a least-squares weighted residual to yield:

$$\left[\mathbf{L}^T\mathbf{W}_1\mathbf{L} + (\mathbf{B}^h)^T\mathbf{W}_2\mathbf{B}^h + (\mathbf{B}^g)^T\mathbf{W}_3\mathbf{B}^g\right]\mathbf{d} = \mathbf{K}^T\mathbf{W}\mathbf{f} \tag{26}$$

where the weighting matrices can be chosen as $\mathbf{W}_1 = \mathbf{I}$, $\mathbf{W}_2 = \sqrt{\alpha^h}\mathbf{I}$, and $\mathbf{W}_3 = \sqrt{\alpha^g}\mathbf{I}$, where $\mathbf{I}$ denotes the identity matrix. It is apparent that the solution of Eq. (26) depends on the Poisson's ratio, and, therefore, the locking can be identified from the first two terms of the LHS.

2.1 Modal analysis

In this section, the modal analysis of a unit square domain with 3 by 3 points is performed to verify the volumetric locking in the RBCM. For simplicity, the unit square domain is considered to be traction-free on all edges, the Young's modulus is unity, and the shape parameter 5 and $Nc = 5 \times 5$ are adopted. The modal analysis presented here is then based on $\mathbf{L}^T\mathbf{W}_1\mathbf{L} + (\mathbf{B}^h)^T\mathbf{W}_2\mathbf{B}^h$ in the LHS of Eq. (26). Figure 1 shows the eigen modes for the case $\nu = 0.4999$. The eigenvalues associated with each mode when ν approaches 0.5 are examined in Fig. 2, in which the horizontal axis is $-\log_{10}(0.5-\nu)$ and the vertical axis is $\log_{10}(Eig.)$. As can be seen, all eigenvalues grow exponentially with $1/(0.5-\nu)$, demonstrating that the RBCM solution locks in the incompressible limit.

Remark 2.1 Due to lack of linear field reproducibility, the three rigid body modes in 2D are not associated with zero eigenvalues. Moreover, while the rotation mode is associated with lowest eigenvalue, the modes close to the two translation modes (Mode 17 and 18) are associated with the two highest eigenvalues in this modal analysis. The linear field reproducibility can be reached if the shape parameter is increased. As a result, the rigid body mode can be better represented with a larger shape parameter. Nevertheless, despite failure of representing rigid body modes, RBCM still offers exceptionally accurate results provided the system is well conditioned.

2.2 Locking of RBCM

The locking of RBCM can also be seen in the following elasticity problem. An infinite long cylinder subjected to an internal pressure is modeled by a 2D quarter model in the first quadrant under plane strain assumption and symmetric boundary condition. The geometry and material property of the cylinder and its RBCM discretization are given in Fig. 3a, b, respectively.

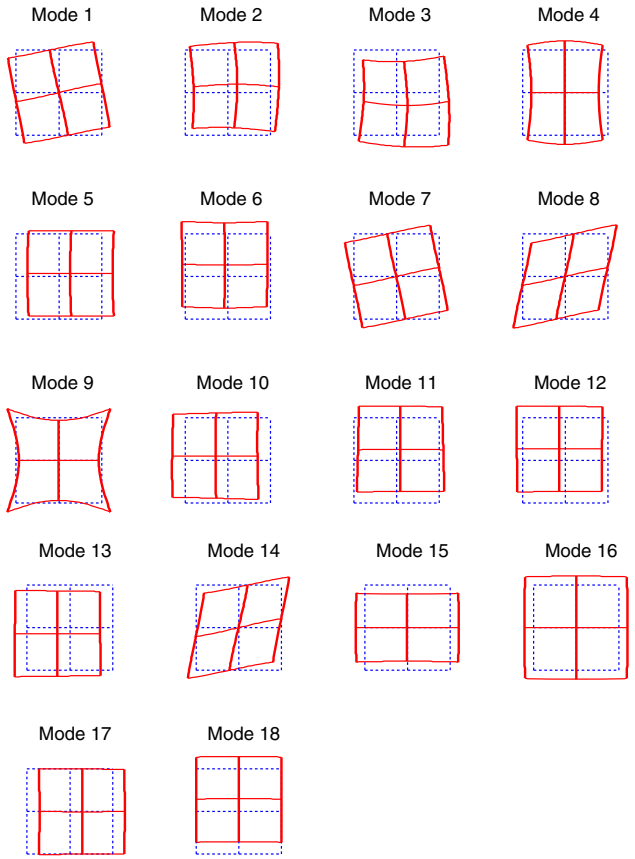

Fig. 1 Eigen modes of RBCM stiffness matrix

Four levels of discretization with 7×7, 9×9, 11×11, and 13×13 radially uniformly distributed source points are performed, and the shape parameters used for each level are 10, 7.5, 6, and 5, respectively. The number of collocation points is $(2N_1-1)\times(2N_2-1)$, where N_i is the number of source points in each direction. The convergence of RBCM in terms of L_2 error norm when ν approaches 0.5 is given in Fig. 4.

Two different selections of $\sqrt{\alpha^g}$ are tested in Fig. 4. Solid lines present the results by using $\sqrt{\alpha^g} \approx O(\mu N s)$ whereas dashed lines present those by $\sqrt{\alpha^g} \approx O(\max(\lambda, \mu)N_s)$. The case with $\sqrt{\alpha^g} \approx O(\mu N_s)$ gives better results and the solution converges with a high rate when v = 0.4999. Therefore, in the elasticity problem, especially nearly incompressible problem, the weight associated with boundary collocation equation should be proportional to shear modulus μ and be independent of ν. Nonetheless, it is evident that for both selections of $\sqrt{\alpha^g}$, locking exists when ν approaches 0.5. The base η of exponential convergence in the form of $\eta^{\frac{d}{H}}$ in (13) shown in Table 1 clearly demonstrates locking behavior

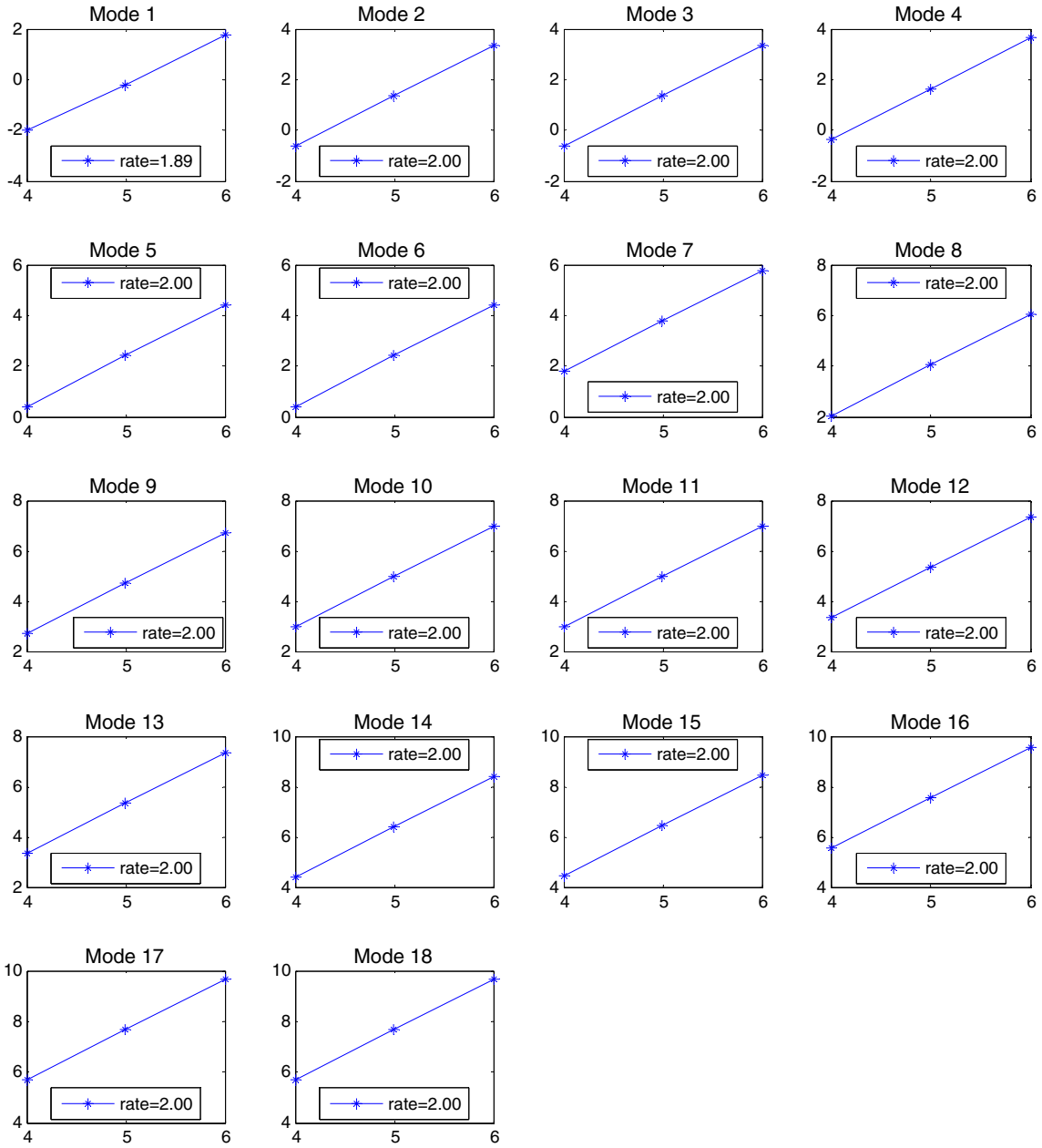

Fig. 2 Eigenvalues as ν approaches 0.5. x-axis is $-\log_{10}(0.5-\nu)$ and y-axis is $\log_{10}(Eig.)$

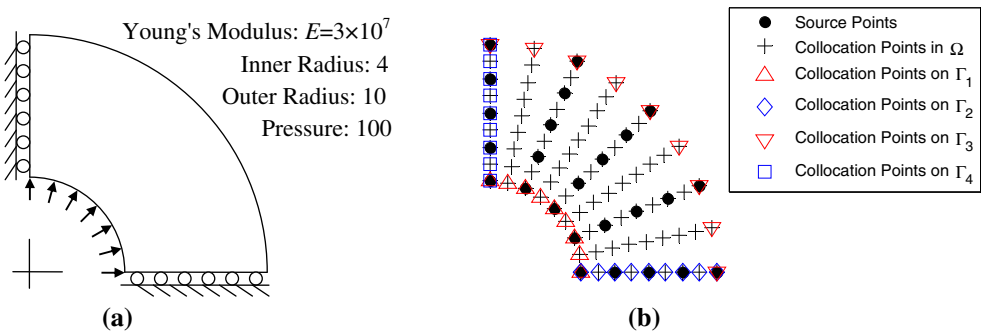

Fig. 3 Problem description and RBCM discretization of an infinite cylinder subjected internal pressure

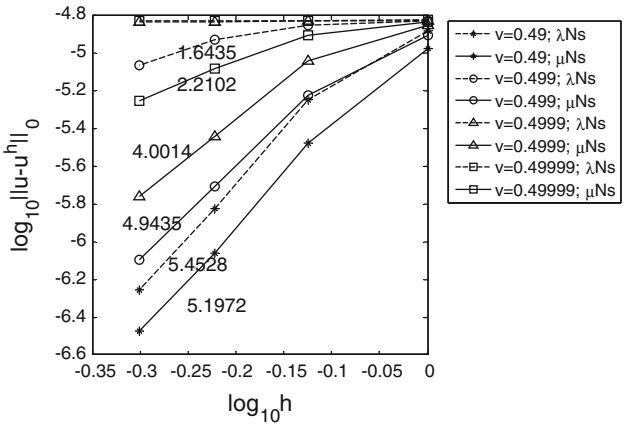

Fig. 4 Convergence of L2 error norm of displacement based RBCM

Table 1 The base η of exponential convergence in RBCM when ν approaches 0.5

	$\nu = 0.49$	$\nu = 0.499$	$\nu = 0.4999$	$\nu = 0.49999$
η	0.56229	0.63201	0.70544	0.84995

in RBCM in the incompressible limit. Hence, an improved formulation to relieve the locking is necessary for RBCM.

3 Mixed formulation for the radial basis collocation method (M-RBCM)

In the limit of incompressibility, the boundary value problem for elasticity is expressed as:

$$(-p\delta_{ij} + 2\mu u_{(i,j)})_{,j} + b_i = 0 \quad \text{in} \quad \Omega \tag{27}$$

$$p/\lambda + u_{i,i} = 0 \quad \text{in} \quad \Omega \tag{28}$$

$$(-p\delta_{ij} + 2\mu u_{(i,j)})n_j = h_i \quad \text{on} \quad \partial\Omega^h \tag{29}$$

$$u_i = g_i \quad \text{on } \partial\Omega^g \tag{30}$$

where $u_{(i,j)}$ is the symmetric gradient of displacement. Note that in the incompressible case p has a physical meaning of hydrostatic pressure, and is necessary for getting a unique solution. In the compressible or nearly incompressible problems, however, p does not carry the meaning of hydrostatic pressure. When $\nu = 0.5$, Eq. (28) becomes the divergence-free constraint $u_{i,i} = 0$.

We let the displacement and pressure fields be approximated by different sets of RBFs $\bar{g}_I$, with the corresponding source points on $\mathbf{T} = [\mathbf{x}_1, \mathbf{x}_2, \ldots \mathbf{x}_{\bar{N}s}] \subseteq \hat{\Omega}$ as:

$$\mathbf{u} \approx \mathbf{u}^h = \sum_{I=1}^{Ns} g_I \mathbf{d}_I \equiv \mathbf{G}\mathbf{d} \tag{31}$$

$$p \approx p^h = \sum_{I=1}^{\bar{N}s} \bar{g}_I \bar{d}_I \equiv \bar{\mathbf{G}}\bar{\mathbf{d}} \tag{32}$$

where $\mathbf{G}$ and $\mathbf{d}$ are defined in (6), and $\bar{\mathbf{G}} = \left[\bar{g}_1, \bar{g}_2, \ldots, \bar{g}_{\bar{N}s}\right]$ and $\bar{\mathbf{d}} = [\bar{d}_1, \bar{d}_2, \ldots, \bar{d}_{\bar{N}s}]^T$. In the Galerkin type mixed formulation, it is well-known that the choice of the bases for different variables is most critical to the accuracy and convergence of the method, and inappropriate combination of bases for different variables could lead to locking or instability. In this approach, on the other hand, the choice of RBFs as the basis functions and the associated source points and shape parameters can be very straightforward due to the employment of a strong form collocation method as to be discussed below.

We now introduce collocation of the equations corresponding to Eqs. (27)–(30) to yield

$$\hat{\mathcal{L}}(\mathbf{G}(\xi_J))\mathbf{d} + \bar{\mathcal{L}}(\bar{\mathbf{G}}(\xi_J))\bar{\mathbf{d}} = \mathbf{f}(\xi_J) \quad \forall \xi_J \in \Omega \tag{33}$$

$$\hat{\mathcal{D}}(\mathbf{G}(\xi_J))\mathbf{d} + \bar{\mathcal{D}}(\bar{\mathbf{G}}(\xi_J))\bar{\mathbf{d}} = 0 \quad \forall \xi_J \in \Omega \tag{34}$$

$$\hat{\mathcal{B}}^h(\mathbf{G}(\xi_J))\mathbf{d} + \bar{\mathcal{B}}^h(\bar{\mathbf{G}}(\xi_J))\bar{\mathbf{d}} = \mathbf{h}(\xi_J) \quad \forall \xi_J \in \partial\Omega^h \tag{35}$$

$$\mathcal{B}^g(\mathbf{G}(\xi_J))\mathbf{d} = \mathbf{g}(\xi_J) \quad \forall \xi_J \in \partial\Omega^g \tag{36}$$

In two dimensional elasticity as an example, the operator matrices $\hat{\mathcal{L}}$, $\bar{\mathcal{L}}$, $\hat{\mathcal{D}}$, $\bar{\mathcal{D}}$, $\hat{\mathcal{B}}^h$, and $\bar{\mathcal{B}}^h$ are

$$\hat{\mathcal{L}} = \begin{bmatrix} 2\mu\frac{\partial^2}{\partial x_1^2} + \mu\frac{\partial^2}{\partial x_2^2} & \mu\frac{\partial^2}{\partial x_1 \partial x_2} \\ \mu\frac{\partial^2}{\partial x_1 \partial x_2} & 2\mu\frac{\partial^2}{\partial x_2^2} + \mu\frac{\partial^2}{\partial x_1^2} \end{bmatrix}, \quad \bar{\mathcal{L}} = \begin{bmatrix} -\frac{\partial}{\partial x_1} \\ -\frac{\partial}{\partial x_2} \end{bmatrix} \tag{37}$$

$$\hat{\mathcal{D}} = \begin{bmatrix} \frac{\partial}{\partial x_1} & \frac{\partial}{\partial x_2} \end{bmatrix}, \quad \bar{\mathcal{D}} = [1/\lambda] \tag{38}$$

$$\hat{\mathcal{B}}^h = \begin{bmatrix} 2\mu n_1 \frac{\partial}{\partial x_1} + \mu n_2 \frac{\partial}{\partial x_2} & \mu n_2 \frac{\partial}{\partial x_1} \\ \mu n_1 \frac{\partial}{\partial x_2} & 2\mu n_2 \frac{\partial}{\partial x_2} + \mu n_1 \frac{\partial}{\partial x_1} \end{bmatrix},$$
$$\bar{\mathcal{B}}^h = \begin{bmatrix} -n_1 \\ -n_2 \end{bmatrix} \tag{39}$$

When the number of source points is larger than that of the collocation points in Eqs.(33)–(36), a least-squares method is applied to obtain the solution. This solution is equivalent to that obtained by the minimization of the following least-squares functional with quadrature [11]:

$$E(\mathbf{v}, q) = \frac{1}{2}\int_{\Omega}^{\wedge} \left(\hat{\mathcal{L}}\mathbf{v} + \bar{\mathcal{L}}q - \mathbf{f}\right)^2 d\Omega + \frac{1}{2}\int_{\Omega}^{\wedge} \left(\hat{\mathcal{D}}\mathbf{v} + \bar{\mathcal{D}}q\right)^2 d\Omega + \frac{1}{2}\int_{\partial\Omega^h}^{\wedge} \left(\hat{\mathcal{B}}^h\mathbf{v} + \bar{\mathcal{B}}^h q - \mathbf{h}\right)^2 d\Gamma + \frac{1}{2}\int_{\partial\Omega^g}^{\wedge} \left(\mathcal{B}^g\mathbf{v} - \mathbf{g}\right)^2 d\Gamma \tag{40}$$

The problem statement is to find $\mathbf{u}^h$ and p^h satisfying:

$$E\left(\mathbf{u}^h, p^h\right) = \inf_{\mathbf{v}\in V, q\in V'} E(\mathbf{v}, q) \tag{41}$$

where V and $V'$are the finite dimensional space spanned by RBFs as given in (31) and (32).

3.1 Weighted M-RBCM

For achieving optimal convergence in solving the collocation equation in (33)–(36) by least-squares method, these four sets of collocation equations need to be properly weighted. Considering the first least-squares term in (40) as the base term, weights for the other three terms in the least-squares functional are applied as follows:

$$\begin{aligned} E(\mathbf{v}, q) = {} & \tfrac{1}{2}\int_{\Omega}^{\wedge}(\hat{\mathcal{L}}\mathbf{v} + \bar{\mathcal{L}}q - \mathbf{f})^2 d\Omega + \tfrac{\alpha^d}{2}\int_{\Omega}^{\wedge}(\hat{\mathcal{D}}\mathbf{v} + \bar{\mathcal{D}}q)^2 d\Omega \\ & + \tfrac{\alpha^h}{2}\int_{\partial\Omega^h}^{\wedge}(\hat{\mathcal{B}}^h\mathbf{v} + \bar{\mathcal{B}}^h q - \mathbf{h})^2 d\Gamma \\ & + \tfrac{\alpha^g}{2}\int_{\partial\Omega^g}^{\wedge}(\mathcal{B}^g\mathbf{v} - \mathbf{g})^2 d\Gamma \end{aligned} \tag{42}$$

Correspondingly, define the following norm:

$$\begin{aligned} \|\mathbf{v}, q\|_B = \Big(& \left\|\hat{\mathcal{L}}\mathbf{v} + \bar{\mathcal{L}}q\right\|_{0,\Omega}^2 + \alpha^d \left\|\hat{\mathcal{D}}\mathbf{v} + \bar{\mathcal{D}}q\right\|_{0,\Omega}^2 \\ & + \alpha^h \left\|\hat{\mathcal{B}}^h\mathbf{v} + \bar{\mathcal{B}}^h q\right\|_{0,\partial\Omega^h}^2 + \alpha^g \left\|\mathcal{B}^g\mathbf{v}\right\|_{0,\partial\Omega^g}^2 \Big)^{1/2} \end{aligned} \tag{43}$$

We have the following error estimate:

$$\begin{aligned} & \|\boldsymbol{u} - \mathbf{v}, p - q\|_B \\ & = \Big(\left\|\hat{\mathcal{L}}\mathbf{v} + \bar{\mathcal{L}}q - \mathbf{f}\right\|_{0,\Omega}^2 + \alpha^d \left\|\hat{\mathcal{D}}\mathbf{v} + \bar{\mathcal{D}}q\right\|_{0,\Omega}^2 \\ & \quad + \alpha^h \left\|\hat{\mathcal{B}}^h\mathbf{v} + \bar{\mathcal{B}}^h q - \mathbf{h}\right\|_{0,\partial\Omega^h}^2 + \alpha^g \left\|\mathcal{B}^g\mathbf{v} - \mathbf{g}\right\|_{0,\partial\Omega^g}^2 \Big)^{1/2} \\ & \le C \Big(\left\|\hat{\mathcal{L}}\mathbf{v} + \bar{\mathcal{L}}q - \mathbf{f}\right\|_{0,\Omega} + \sqrt{\alpha^d}\left\|\hat{\mathcal{D}}\mathbf{v} + \bar{\mathcal{D}}q\right\|_{0,\Omega} \\ & \quad + \sqrt{\alpha^h}\left\|\hat{\mathcal{B}}^h\mathbf{v} + \bar{\mathcal{B}}^h q - \mathbf{h}\right\|_{0,\partial\Omega^h} + \sqrt{\alpha^g}\left\|\mathcal{B}^g\mathbf{v} - \mathbf{g}\right\|_{0,\partial\Omega^g} \Big) \\ & = C \Big(\left\|\hat{\mathcal{L}}\mathbf{v} + \bar{\mathcal{L}}q - \hat{\mathcal{L}}\mathbf{u} - \bar{\mathcal{L}}p\right\|_{0,\Omega} \\ & \quad + \sqrt{\alpha^d}\left\|\hat{\mathcal{D}}\mathbf{v} + \bar{\mathcal{D}}q - \hat{\mathcal{D}}\mathbf{u} - \bar{\mathcal{D}}p\right\|_{0,\Omega} \\ & \quad + \sqrt{\alpha^h}\left\|\hat{\mathcal{B}}^h\mathbf{v} + \bar{\mathcal{B}}^h q - \hat{\mathcal{B}}^h\mathbf{u} - \bar{\mathcal{B}}^h p\right\|_{0,\partial\Omega^h} \\ & \quad + \sqrt{\alpha^g}\left\|\mathcal{B}^g\mathbf{v} - \mathcal{B}^g\mathbf{u}\right\|_{0,\partial\Omega^g} \Big) \end{aligned} \tag{44}$$

With further manipulation, we have

$$\begin{aligned} & \|\mathbf{u} - \mathbf{v}, p - q\|_B \\ & \le C_1\left\|\hat{\mathcal{L}}(\mathbf{v} - \mathbf{u})\right\|_{0,\Omega} + C_2\left\|\bar{\mathcal{L}}(q - p)\right\|_{0,\Omega} \\ & \quad + C_3\sqrt{\alpha^d}\left\|\hat{\mathcal{D}}(\mathbf{v} - \mathbf{u})\right\|_{0,\Omega} + C_4\sqrt{\alpha^d}\left\|\bar{\mathcal{D}}(q - p)\right\|_{0,\Omega} \\ & \quad + C_5\sqrt{\alpha^h}\left\|\hat{\mathcal{B}}^h(\mathbf{v} - \mathbf{u})\right\|_{0,\partial\Omega^h} + C_6\sqrt{\alpha^h}\left\|\bar{\mathcal{B}}^h(q - p)\right\|_{0,\partial\Omega^h} \\ & \quad + C_7\sqrt{\alpha^g}\left\|\mathcal{B}^g(\mathbf{v} - \mathbf{u})\right\|_{0,\partial\Omega^g} \\ & \le C_1\mu\|\mathbf{v} - \mathbf{u}\|_{2,\Omega} + C_2\|q - p\|_{1,\Omega} + C_3\sqrt{\alpha^d}\|\mathbf{v} - \mathbf{u}\|_{1,\Omega} \\ & \quad + C_4\frac{\sqrt{\alpha^d}}{\lambda}\|q - p\|_{0,\Omega} \\ & \quad + C_5\mu\sqrt{\alpha^h}\|\mathbf{v} - \mathbf{u}\|_{1,\partial\Omega^h} + C_6\sqrt{\alpha^h}\|q - p\|_{0,\partial\Omega^h} \\ & \quad + C_7\sqrt{\alpha^g}\|\mathbf{v} - \mathbf{u}\|_{0,\partial\Omega^g} \end{aligned} \tag{45}$$

Here we introduce the following inequalities:

$$\begin{aligned} & \|\mathbf{v} - \mathbf{u}\|_{1,\partial\Omega^h} \le C\|\mathbf{v} - \mathbf{u}\|_{2,\Omega} \\ & \|\mathbf{v} - \mathbf{u}\|_{0,\partial\Omega^g} \le C\|\mathbf{v} - \mathbf{u}\|_{1,\Omega} \\ & \|q - p\|_{0,\partial\Omega^h} \le C\|q - p\|_{1,\Omega} \\ & \|\mathbf{v} - \mathbf{u}\|_{1,\Omega} \le CN_S^{-1}\|\mathbf{v} - \mathbf{u}\|_{2,\Omega} \\ & \|q - p\|_{0,\Omega} \le CN_S^{-1}\|q - p\|_{1,\Omega} \end{aligned} \tag{46}$$

By introducing (46) into (45), we obtain the following error bound:

$$\begin{aligned} & \|\mathbf{u} - \mathbf{v}, p - q\|_B \\ & \le C_1\mu\|\mathbf{v} - \mathbf{u}\|_{2,\Omega} + C_2\|q - p\|_{1,\Omega} + C_3\sqrt{\alpha^d}\|\mathbf{v} - \mathbf{u}\|_{1,\Omega} \\ & \quad + C_4\frac{\sqrt{\alpha^d}}{\lambda}\|q - p\|_{0,\Omega} + C_5\mu\sqrt{\alpha^h}\|\mathbf{v} - \mathbf{u}\|_{1,\partial\Omega^h} \\ & \quad + C_6\sqrt{\alpha^h}\|q - p\|_{0,\partial\Omega^h} + C_7\sqrt{\alpha^g}\|\mathbf{v} - \mathbf{u}\|_{0,\partial\Omega^g} \\ & \le \left(C_1\mu + \frac{C_3}{N_S}\sqrt{\alpha^d} + C_5\mu\sqrt{\alpha^h} + \frac{C_7}{N_S}\sqrt{\alpha^g}\right)\|\mathbf{v} - \mathbf{u}\|_{2,\Omega} \\ & \quad + \left(C_2 + C_4\frac{\sqrt{\alpha^d}}{\lambda N_S} + C_6\sqrt{\alpha^h}\right)\|q - p\|_{1,\Omega} \end{aligned} \tag{47}$$

Imposing error balance in the domain and boundary terms in the $\|\,\|_B$ norm and considering $\boldsymbol{\lambda >> \mu}$, we obtain

$$\begin{aligned} & \sqrt{\alpha^d} \approx O(\mu N_s) \\ & \sqrt{\alpha^h} \approx O(1) \\ & \sqrt{\alpha^g} \approx O(\mu N_s) \end{aligned} \tag{48}$$

The optimal solution $(\mathbf{u}^h, p^h)$ has the following error bound:

$$\left\|\mathbf{u} - \mathbf{u}^h, p - p^h\right\|_B \le \bar{C}_1\|\mathbf{v} - \mathbf{u}\|_{2,\Omega} + \bar{C}_2\|q - p\|_{1,\Omega} \tag{49}$$

Remark 3.1 The norm $\|\cdot\|_B$ is equivalent to 2-norm of the solution:

$$\|\mathbf{u}, p\|_B = \|\mathbf{u}\|_{2,\Omega} + \|p\|_{1,\Omega} \tag{50}$$

Thus the error is bounded by

$$\left\|\mathbf{u} - \mathbf{u}^h, p - p^h\right\|_B \le C_1'\eta_u^{a/H}|\mathbf{u}|_t + C_2'\eta_p^{a/H}|p|_t \tag{51}$$

where $0<\eta_u, \eta_p<1$, H is the averaged distance between source points, and a is the shape parameter of RBF. Since $\|\mathbf{u}-\mathbf{v}\|_{1,\Omega} \leq C_1 N_S^{-1} \|\mathbf{u}-\mathbf{v}\|_{2,\Omega}$ and $\|p-q\|_{0,\Omega} \leq C_2 N_S^{-1} \|p-q\|_{1,\Omega}$, we have the following error estimate:

$$\|\mathbf{u}-\mathbf{v}\|_{1,\Omega} + \|p-q\|_{0,\Omega} \leq C N_S^{-1} (\|\mathbf{u}-\mathbf{v}\|_{2,\Omega} + \|p-q\|_{1,\Omega}) \tag{52}$$

where $C = \max\{C_1, C_2\}$. Thus, we have

$$\left\|\mathbf{u}-\mathbf{u}^h\right\|_{1,\Omega} + \left\|p-p^h\right\|_{0,\Omega} \leq C_1'' \bar{\eta}_u^{a/H} |\mathbf{u}|_t + C_2'' \bar{\eta}_p^{a/H} |p|_t \tag{53}$$

where $\bar{\eta}_u = e^{\frac{2H}{a} \ln H + \ln \eta_u}$ satisfying $0 < \bar{\eta}_u < \eta_u < 1$, and $\bar{\eta}_p = e^{\frac{2H}{a} \ln H + \ln \eta_p}$ satisfying $0 < \bar{\eta}_p < \eta_p < 1$. This result shows that the numerical solution $(\mathbf{u}^h, p^h)$ converges exponentially to $(\mathbf{u}, p)$ as the model is refined.

Remark 3.2 In the Galerkin method, the pressure-displacement mixed formulation leads to a saddle point problem. Improper combination of pressure and displacement approximations yields either locking or instability in the form of pressure oscillation. In contrast, the RBCM overdetermined system of collocation equations solved by a least-squares method resembles a minimization problem. This convexity in the discrete system offers stability to the solution and allows a less restrictive choice of displacement and pressure basis functions for locking avoidance.

Remark 3.3 Based on the equivalence between the minimization of discretized least-squares functional with quadrature and collocation equations solved by the least-squares method, the corresponding collocation equations of the minimization of the discretized weighted least-squares functional (42) is

$$\hat{\mathcal{L}}(\mathbf{G}(\xi_J))\mathbf{d} + \bar{\mathcal{L}}(\bar{\mathbf{G}}(\xi_J))\,\bar{\mathbf{d}} = \mathbf{f}(\xi_J) \quad \forall \xi_J \in \Omega \tag{54}$$

$$\sqrt{\alpha^d}\hat{\mathcal{D}}(\mathbf{G}(\xi_J))\mathbf{d} + \sqrt{\alpha^d}\bar{\mathcal{D}}(\bar{\mathbf{G}}(\xi_J))\,\bar{\mathbf{d}} = 0 \quad \forall \xi_J \in \Omega \tag{55}$$

$$\sqrt{\alpha^h}\hat{\mathcal{B}}^h(\mathbf{G}(\xi_J))\mathbf{d} + \sqrt{\alpha^h}\bar{\mathcal{B}}^h(\bar{\mathbf{G}}(\xi_J))\,\bar{\mathbf{d}} = \sqrt{\alpha^h}\mathbf{h}(\xi_J) \quad \forall \xi_J \in \partial\Omega^h \tag{56}$$

$$\sqrt{\alpha^g}\mathcal{B}^g(\mathbf{G}(\xi_J))\mathbf{d} = \sqrt{\alpha^g}\mathbf{g}(\xi_J) \quad \forall \xi_J \in \partial\Omega^g \tag{57}$$

4 Numerical examples

In this section, we present some numerical examples to demonstrate the capabilities of the proposed M-RBCM, and, in particular, to verify the robustness of M-RBCM in the incompressible limit. The convergence behaviors of M-RBCM are compared with pure displacement based RBCM in terms of L_2 norm and H_1semi-norm defined as follows.

$$\left\|\mathbf{u}-\mathbf{u}^h\right\|_0 = \left(\int_\Omega (u_i - u_i^h)(u_i - u_i^h)d\Omega\right)^{1/2} \tag{58}$$

$$\left|\mathbf{u}-\mathbf{u}^h\right|_1 = \left(\int_\Omega (u_{i,j} - u_{i,j}^h)(u_{i,j} - u_{i,j}^h)d\Omega\right)^{1/2} \tag{59}$$

In the following study, IMQ RBFs are used for the approximation of displacement and pressure fields. The source points and the RBF shape factors for both fields are chosen to be the same for both approximations. The weights for the weighted RBCM $\sqrt{\alpha^d} = \mu Ns$, $\sqrt{\alpha^h} = 1$, and $\sqrt{\alpha^g} = \mu Ns$ are employed for the incompressibility constraint, Neumann boundary, and Dirichlet boundary collocation equations, respectively, where Ns is the total number of source points.

4.1 An infinite long cylinder subjected to an internal pressure

The same model problem presented in Fig. 3 is revisited by using M-RBCM method in this section. For simplicity, the same set of RBFs (IMQ) is adopted for both displacement and pressure fields. Similarly, four levels of discretization with 7×7, 9×9, 11×11, and 13×13 source points are performed, and the shape parameters used associated with each level of discretization are 10, 7.5, 6, and 5, respectively. Also the same set of $(2N_1-1)\times(2N_2-1)$ collocation points is used for both Eqs. (54) and (55). The collocation points located on the boundaries are used as the collocation points for the two sets of boundary collocation equations in (56) and (57).

The convergence behaviors of M-RBCM are compared with the pure displacement based RBCM in Fig. 5a, b, in terms of L_2 norm and H_1 semi-norm, respectively. For compressible case ($\nu = 0.25$), solutions from M-RBCM are more accurate than those from RBCM. The convergence rates obtained from M-RBCM are slightly higher than those from RBCM in both L_2 norm and H_1 semi-norm. For the incompressible case ($\nu = 0.5$), M-RBCM has the same exponential convergence as shown in the compressible case, which indicates no locking is observed in M-RBCM. On the other hand, RBCM suffers from locking and experiences a lower convergence rate when Poisson's ratio approaches 0.5 ($\nu = 0.4999$). The base η of exponential convergence in the form of $\eta^{\frac{a}{H}}$ described in *Remark* 3.1 for both L_2 and H_1 semi-norms are shown in Table 2. The results again conform that the locking in RBCM is avoided in M-RBCM. Figure 6a, b show the solutions of stresses σ_{rr}, $\sigma_{\theta\theta}$, and pressure p using 11×11 source points obtained by M-RBCM and RBCM, respectively. The numerical results of M-RBCM agree well with analytical ones and no pressure oscillation is observed, whereas those of RBCM have noticeable disagreements from analytical ones.

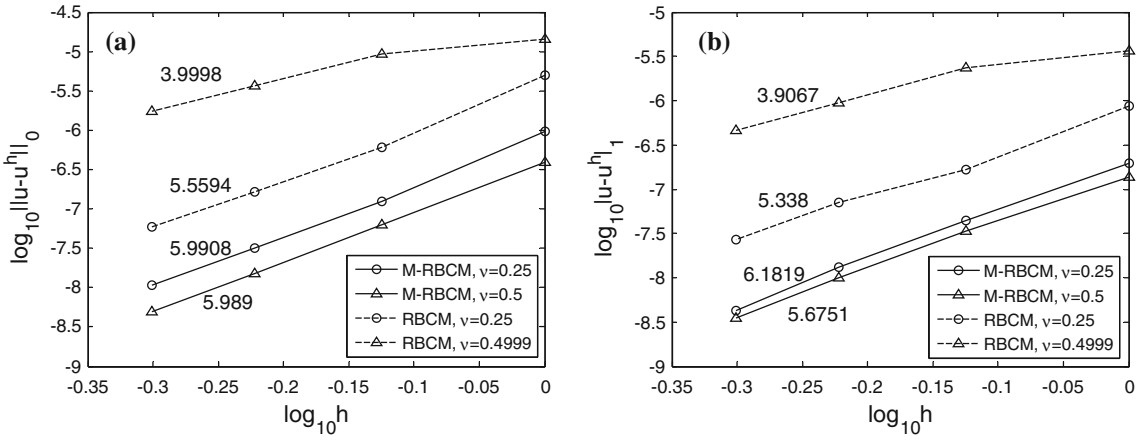

Fig. 5 Convergence of L2 norm and H1 semi-norm for cylinder problem

Table 2 The base η of exponential convergence in the cylinder problem

		M-RBCM		RBCM	
		$\nu = 0.25$	$\nu = 0.5$	$\nu = 0.25$	$\nu = 0.4999$
η	L_2	0.46733	0.48353	0.47853	0.70544
	H_1	0.52611	0.54230	0.56110	0.70884

4.2 Beam bending

A cantilever beam with length $L = 10$ and height $D = 2$ subjected to a parabolic shear traction at the right end shown in Fig. 7a is analyzed. The resultant of the shear traction is $P = 100$, the Young's modulus of the beam is $E = 3 \times 10^7$, and the plane strain condition is assumed. The domain is discretized uniformly with RBFs as shown in Fig. 7b. Three levels of discretization with 11×3, 16×4, 26×6 source points are performed in the convergence study. The shape parameters for each level of discretization are 30, 20, and 12, respectively. A total of $(2N_1 - 1) \times (2N_2 - 1)$ collocation points are used for both Eqs. (54) and (55), which correspond to 21×5, 31×7, and 51×11 collocation points. The collocation points located on the boundaries are used as the collocation points for the two sets of boundary collocation equations in (56) and (57).

The specific boundary conditions imposed are given as follows:

$$
\begin{array}{ll}
h_i = 0 & \text{on } 0 \le x \le L,\ y = \pm D/2 \\
h_1 = 0,\ h_2 = \frac{P}{8I}(D^2 - 4y^2) & \text{on } x = L,\ -D/2 \le y \le D/2 \\
h_1 = 0,\ h_2 = -\frac{P}{8I}(D^2 - 4y^2) & \text{on } x = 0,\ -D/2 < y < 0,\ 0 < y < D/2 \\
g_1 = 0,\ h_2 = 0 & \text{at } x = 0,\ y = \pm D/2 \\
g = 0,\ g_2 = 0 & \text{at } x = 0,\ y = 0
\end{array}
\tag{60}
$$

The analytical solution of this problem [53] is:

$$u_1 = -\frac{Py}{6\bar{E}I}\left[(6L - 3x)x + (2 + \bar{\nu})\left(y^2 - \frac{D^2}{4}\right)\right]$$

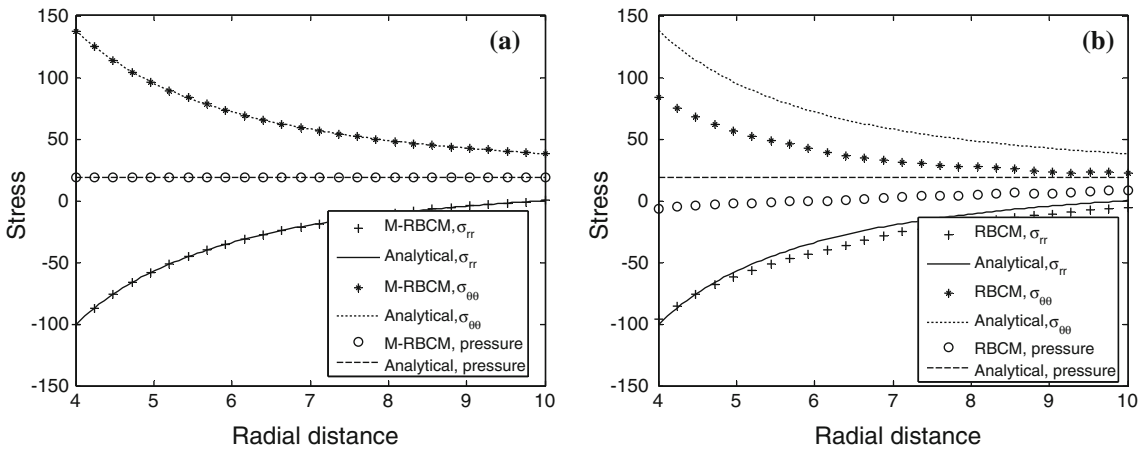

Fig. 6 Stress solutions of cylinder problem obtained by **a** M-RBCM and **b** RBCM

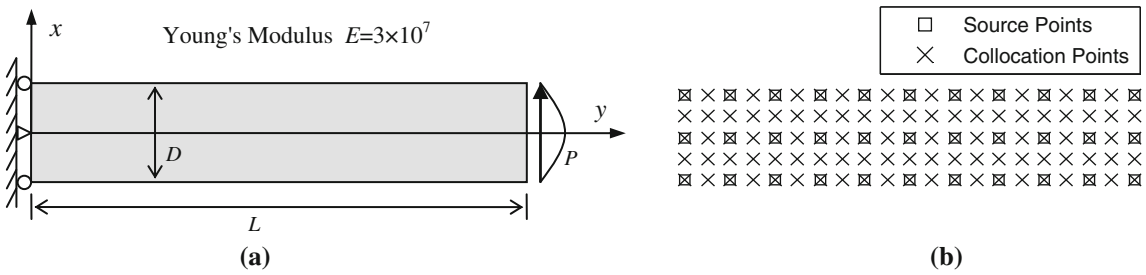

Fig. 7 Problem description and RBCM discretization of cantilever beam

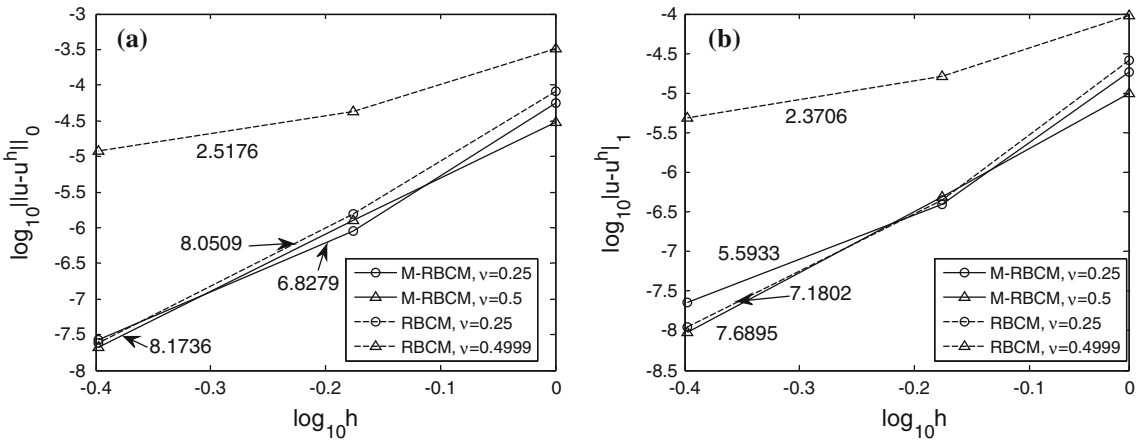

Fig. 8 Convergence of L2 norm and H1 semi-norm of beam problem

$$u_2 = \frac{P}{6\bar{E}I}\left[(3L-x)x^2 + 3\bar{\nu}y^2(L-x) + (4+5\bar{\nu})\frac{D^2x}{4}\right] \tag{61}$$

where P is the resultant of the shear traction, $I = D^3/12$, $\bar{E} = E/(1-\nu^2)$, and $\bar{\nu} = \nu/(1-\nu)$.

Figure 8a, b compare the convergence behaviors of M-RBCM with RBCM in the L_2 norm and H_1 semi-norm, respectively. The solutions from M-RBCM have the same level of accuracy and similar rate of convergence for both $\nu = 0.25$ and $\nu = 0.5$ cases, indicating that the M-RBCM is robust in the incompressible limit, whereas the RBCM yields lower rate of convergence when $\nu = 0.4999$. The base η of exponential convergence in the form of $\eta^{\frac{a}{H}}$ as described in *Remark* 3.1 for both L_2 and H_1 semi-norms are shown in Table 3. The results clearly indicate that the locking in RBCM has been corrected in M-RBCM. Figure 9a, b compare solutions of u_1 along $y = 0$ and σ_{12} along $x = L/2$ obtained by M-RBCM with $\nu = 0.5$ and RBCM with $\nu = 0.4999$ using 26×6 source points. Both displacement and stress numerical results obtained by both methods agree well with the analytical solutions, although the ones from M-RBCM show better accuracy than those from RBCM. In particular, the stress solutions from both methods are smooth without oscillation in this problem.

Table 3 The base η of exponential convergence in the beam problem

		M-RBCM		RBCM	
		$\nu = 0.25$	$\nu = 0.5$	$\nu = 0.25$	$\nu = 0.4999$
η	L_2	0.07809	0.08816	0.06608	0.33004
	H_1	0.10796	0.09837	0.07585	0.36917

4.3 Fully constrained block

A fully constrained block in the domain $\Omega = (-\pi/2, \pi/2) \times (-\pi/2, \pi/2)$ subjected to a body force is studied (cf. [44]). This study is aimed to examine the pressure oscillation, typically observed in a highly confined incompressible problem, using the proposed method. The problem setting is depicted in Fig. 10a and its RBCM discretization is given in Fig. 10b. The material properties are assumed to be fully incompressible with shear modulus $\mu = 10^4$. The specific boundary conditions imposed are listed at follows:

$$\begin{aligned} u_i &= 0 \quad \text{on } x = \pm\pi/2 \\ u_i &= 0 \quad \text{on } y = \pm\pi/2 \\ \sigma_{ii}/3 &= 0 \quad \text{at } (0, -\pi/2) \end{aligned} \tag{62}$$

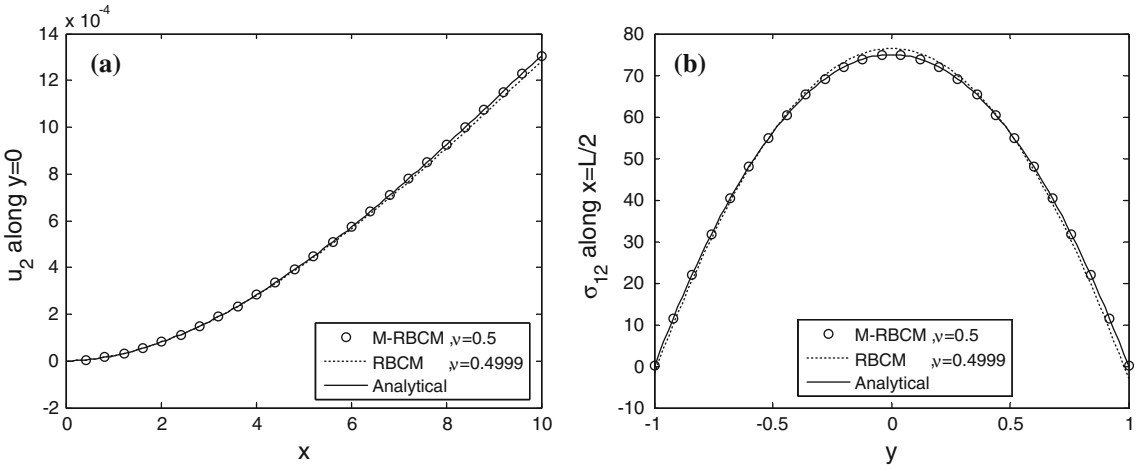

Fig. 9 Displacement and stress solutions of beam problem

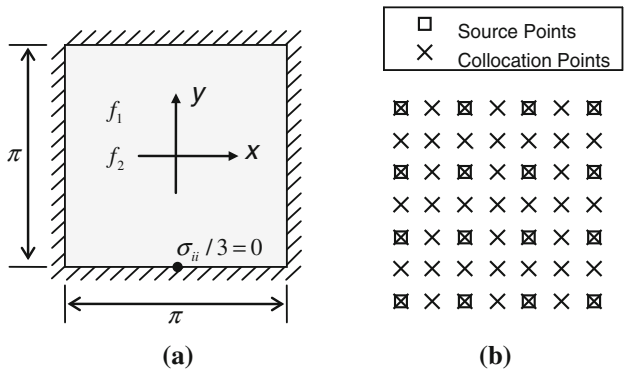

Fig. 10 Problem description and RBCM discretization of fully constrained block

Further, the following body force is selected:

$$f_1 = \mu(\cos y)(\sin y)(1 - 4\cos^2 x) - 2xy(\cos(x^2 y))$$
$$f_2 = -\mu(\cos x)(\sin x)(1 - 4\cos^2 y) - x^2(\cos(x^2 y)) \quad (63)$$

The corresponding analytical solution is

$$u_1 = -(\cos^2 x)(\cos y)(\sin y)/2$$
$$u_2 = (\cos^2 y)(\cos x)(\sin x)/2 \quad (64)$$

Since the problem is incompressible with a fully constrained boundary, it is necessary to prescribe the pressure at one point in the domain. A zero pressure is prescribed at $x = (0, -\pi/2)$, and the corresponding analytical stress solutions are:

$$\sigma_{11} = 2\mu(\cos x)(\cos y)(\sin x)(\sin y)$$
$$\sigma_{22} = -2\mu(\cos x)(\cos y)(\sin x)(\sin y)$$
$$\sigma_{12} = \mu\left[-(\cos^2 x)(-1/2 + \cos^2 y) + (\cos^2 y)(-1/2 + \cos^2 x)\right] \quad (65)$$

Four levels of discretization with 4×4, 6×6, 8×8, and 10×10 source points are performed in the convergence study. The shape parameters used associated with each level of discretization are 35/3, 35/5, 35/7, and 35/9, respectively. The same set of $(2N_1 - 1) \times (2N_2 - 1)$ collocation points is adopted for both domain and constraint equations, which corresponds to 7×7, 11×11, 15×15, and 19×19 collocation points.

The convergence of M-RBCM is compared with that of RBCM in terms of L_2 norm and H_1 semi-norm in Fig. 11. The rates of convergence of M-RBCM are higher for both error norms although both methods show exponential convergence in this problem. Figure 12a shows the horizontal displacement solution along $y = 0$ obtained from M-RBCM. As can be seen, the M-RKCM displacement solution agrees well with the analytical solution, indicating no volumetric locking. The M-RKCM stress and pressure solutions along $x = y$ using 10×10 source points are given in Fig. 12b. Both normal stresses as well as the pressure solution are smooth and in good agreement with the analytical solution. No pressure oscillation or checkerboard pattern appears in the solutions.

4.4 Driven cavity problem

The driven cavity described in Fig. 13a is a commonly studied problem for Stocks flow. Although the analytical solution is not available, we present it here to demonstrate that a smooth pressure field can be obtained by using M-RBCM. This problem is governed by the same boundary value problem stated in Eqs. (27)–(30), with a different physical interpretation. In Stocks flow, u is the velocity fluid, μ is the viscosity, and p is the hydrostatic pressure. The fluid along edges of the domain remains stationary, except along the top with $u = 1$. Note that the x-velocity is discontinuous near the top corners. To make a fair comparison to FEM results, we adopt a linear

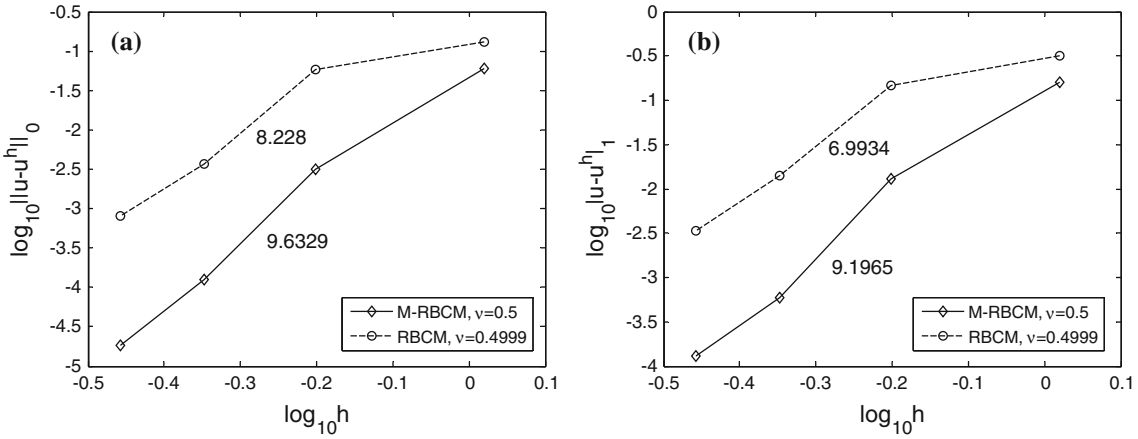

Fig. 11 Convergence of L2 norm and H1 semi-norm and displacement solution of fully constrained problem

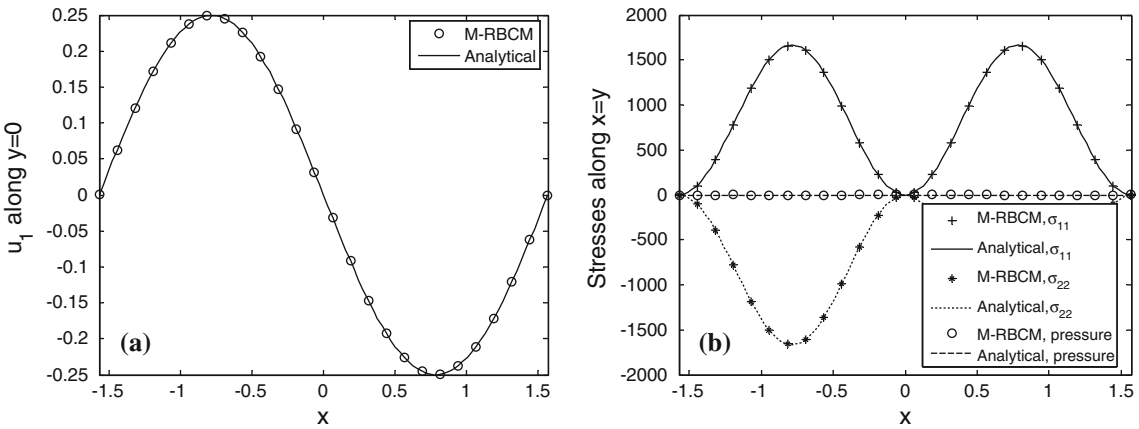

Fig. 12 M-RKCM solutions of fully constrained problem

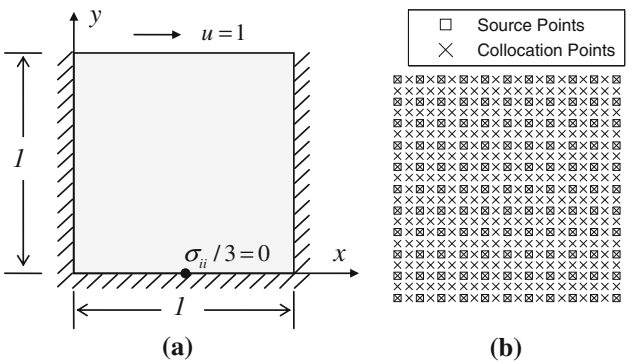

Fig. 13 Problem description and RBCM discretization of driven cavity problem

variation of x-velocity near the top corners, as described in Eq. (67). The material is assumed fully incompressible with unit viscosity. The pressure at the center of the button edge is set to be zero in order to have a unique solution. The detail of boundary conditions used in the example is given as follows.

$$\begin{array}{ll} u_i = 0 & \text{on } 0 < x < 1,\ y = 0 \\ u_1 = \delta(y),\ u_2 = 0 & \text{on } x = 0 \text{ and } 1,\ 0 \le y < 1 \\ u_1 = 1,\ \ u_2 = 0 & \text{on } 0 \le x \le 1,\ y = 1 \\ \sigma_{ii}/3 = 0 & \text{at } x = 1/2,\ y = 0 \end{array} \tag{66}$$

where

$$\delta(y) = \begin{cases} (y - 0.9)/0.1 & 0.9 < y < 1 \\ 0 & 0 \le y \le 0.9 \end{cases} \tag{67}$$

The domain is discretized by RBF with 11×11 source points and 21×21 collocation points as shown in Fig. 13b. The shape parameters used for both displacement and pressure fields are 1.

The pressure contour in the undeformed configuration is shown in Fig. 14a. As can be seen, the pressure solution of M-RBCM is smooth throughout the domain. Figure 14b shows the pressure solution along $y = 0.35$ (cf. [33,54]) and $y = 0.5$ (cf. [55]) in comparison with the solutions obtained from bilinear-displacement constant-pressure M-FEM (4D-1P) [33,54]. No oscillation is observed in M-

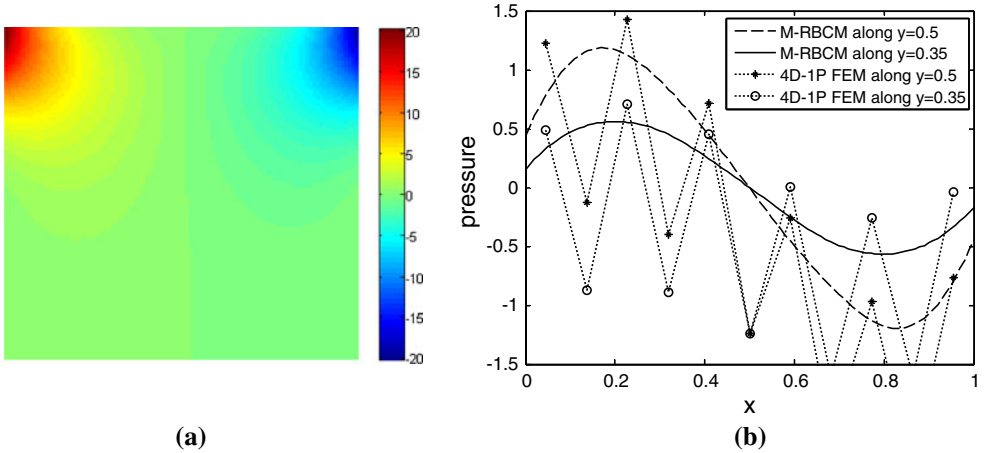

(a) **(b)**

Fig. 14 Pressure solutions of driven cavity problem

RBCM results, while significant pressure oscillation appears in M-FEM solutions.

5 Conclusions

While RBCM has been applied to a wide range of boundary value problems, the modal analysis shows that this method of strong form collocation with displacement field approximated by the radial basis functions yields volumetric locking in that all eigenvalues grow exponentially when the Poisson's ratio approaches 0.5. Proper correction of the weights associated with the boundary collocation equations in RBCM, which has given enhanced convergence of RBCM in other type of boundary value problems, only marginally relieves the locking in RBCM in the limit of incompressibility. We therefore introduce RBCM with pressure and displacement fields independently approximated by radial basis functions for incompressible and nearly incompressible problems, termed M-RBCM. Similar to RBCM, an essential step for M-RBCM to achieve optimal convergence, the errors resulting from collocation equations associated with PDE, the boundary conditions, and the incompressibility constraint must be balanced. This is achieved by introducing appropriate weights to the four sets of collocation equations through error analysis.

Since the strong form collocation in M-RBCM is solved by a least-squares method when the number of collocation is chosen to be greater than source points for better accuracy, the M-RBCM remains a minimization problem rather than a saddle point problem in the Galerkin based mixed formulation. Hence, the choice of basis functions for the displacement and pressure fields is not subjected to the LBB stability condition [29,30]. As shown in the numerical example, the same set of RBFs can be used for both displacement and pressure fields for implementation simplicity. Further, the same set of source points and shape parameters for both displacement and pressure fields can also be employed for simplicity while maintaining accuracy in the proposed M-RBCM. The numerical investigation shows that the L_2 norm and H_1 semi-norm exhibit about the same level of accuracy with extremely high convergence rates. No locking has been observed in the numerical study, even in a fully constrained problem. In addition, pressure oscillation and the notorious checkerboard pattern were absent in the numerical tests. The proposed M-RBCM offers a very accurate and robust solution for the incompressible and nearly incompressible problems. The fact that the same set of basis functions can be used for displacement and pressure variables without encountering locking and pressure oscillation in incompressible problems makes this proposed method more attractive than other Galerkin type mixed formulations.

Acknowledgments The support of this work by the University of Illinois at Chicago to the first author, the support by US Army ERDC under contract W912HZ-07-C-0019 to the second author, and the support by National Science Council (Taiwan) 100-2115-M-029-002 to the third author are greatly acknowledged.

References

1. Belytschko T, Lu YY, Gu L (1994) Element-free Galerkin methods. Int J Numer Method Eng 37(2):229–256
2. Liu WK, Jun S, Zhang YF (1995) Reproducing Kernel particle methods. Int J Numer Method Fluid 20(8–9):1081–1106
3. Babuska I, Melenk JM (1997) The partition of unity method. Int J Numer Method Eng 40(4):727–758
4. Gingold RA, Monaghan JJ (1977) Smoothed particle hydrodynamics—theory and application to non-spherical stars. Mon Notices R Astron Soc 181(2):375–389

5. Atluri SN, Zhu TL (2000) The meshless local Petrov-Galerkin (MLPG) approach for solving problems in elasto-statics. Comput Mech 25(2–3):169–179
6. Chen JS, Pan CH, Wu CT, Liu WK (1996) Reproducing kernel particle methods for large deformation analysis of non-linear structures. Comput Method Appl Mech Eng 139(1–4):195–227
7. Kansa EJ (1990) Multiquadrics—a scattered data approximation scheme with applications to computational fluid-dynamics.1. Comput Math Appl 19(8–9):127–145
8. Kansa EJ (1990) Multiquadrics—a scattered data approximation scheme with applications to computational fluid-dynamics.2. Solutions to parabolic, hyperbolic and elliptic partial-differential equations. Comput Math Appl 19(8–9):147–161
9. Aluru NR (2000) A point collocation method based on reproducing kernel approximations. Int J Numer Method Eng 47(6):1083–1121
10. Hu HY, Chen JS, Hu W (2011) Error analysis of collocation method based on reproducing Kernel approximation. Numer Method Partial Differ Equ 27(3):554–580
11. Chen JS, Hu HY, Hu W (2007) Weighted radial basis collocation method for boundary value problems. Int J Numer Method Eng 69(13):2736–2757
12. Chen JS, Wang LH, Hu HY, Chi SW (2009) Subdomain radial basis collocation method for heterogeneous media. Int J Numer Method Eng 80(2):163–190
13. Franke C, Schaback R (1998) Solving partial differential equations by collocation using radial basis functions. Appl Math Comput 93(1):73–82
14. Hu HY, Li ZC, Cheng AHD (2005) Radial basis collocation methods for elliptic boundary value problems. Comput Math Appl 50(1–2):289–320
15. Wendland H (1999) Meshless Galerkin methods using radial basis functions. Math Comput 68(228):1521–1531
16. Cecil T, Qian JL, Osher S (2004) Numerical methods for high dimensional Hamilton-Jacobi equations using radial basis functions. J Comput Phys 196(1):327–347
17. Pollandt R (1997) Solving nonlinear differential equations of mechanics with the boundary element method and radial basis functions. Int J Numer Method Eng 40(1):61–73
18. Sonar T (1996) Optimal recovery using thin plate splines in finite volume methods for the numerical solution of hyperbolic conservation laws. Ima J Numer Anal 16(4):549–581
19. Chi SW, Chen JS, Luo H, Hu HY, Wang L (2012) Dispersion and stability properties of radial basis collocation method for elastodynamics. In: Numerical methods for partial differential equations. Springer, New York
20. Wang LH, Chen JS, Hu HY (2010) Subdomain radial basis collocation method for fracture mechanics. Int J Numer Method Eng 83(7):851–876
21. Wendland H (1998) Error estimates for interpolation by compactly supported radial basis functions of minimal degree. J Approx Theory 93(2):258–272
22. Chen JS, Hu W, Hu HY (2008) Reproducing kernel enhanced local radial basis collocation method. Int J Numer Method Eng 75(5):600–627
23. Herrmann LR (1965) Elasticity equations for incompressible and nearly incompressible materials by a variational theorem. AIAA J 3(10):1896–1900
24. Murakawa H, Atluri SN (1979) inite elasticity solutions using hybrid finite-elements based on a complementary energy principle.2. Incompressible materials. J Appl Mech Trans ASME 46(1):71–77
25. Pian THH, Sumihara K (1984) Rational approach for assumed stress finite-elements. Int J Numer Method Eng 20(9):1685–1695
26. Simo JC, Rifai MS (1990) A class of mixed assumed strain methods and the method of incompatible modes. Int J Numer Method Eng 29(8):1595–1638
27. Liu WK, Belytschko T, Chen JS (1988) Nonlinear versions of flexurally superconvergent elements. Comput Method Appl Mech Eng 71(3):241–258
28. Chen JS, Satyamurthy K, Hirschfelt LR (1994) Consistent finite-element procedures for nonlinear rubber elasticity with a higher-order strain-energy function. Comput Struct 50(6):715–727
29. Babuska I (1973) Finite-element method with Lagrangian multipliers. Numer Math 20(3):179–192
30. Brezzi F (1974) Existence, uniqueness and approximation of Saddle-point problems arising from Lagrangian multipliers. Revue Francaise D Automatique Informatique Recherche Operationnelle 8(Nr2): 129–151
31. Sani RL, Gresho PM, Lee RL, Griffiths DF (1981) The cause and cure (questionable) of the spurious pressures generated by certain fem solutions of the incompressible Navier-stokes equations.1. Int J Numer Method Fluid 1(1):17–43
32. Sussman T, Bathe KJ (1987) A finite-element formulation for nonlinear incompressible elastic and inelastic analysis. Comput Struct 26(1–2):357–409
33. Hughes TJR (2000) The finite element method: linear static and dynamic finite element analysis. Dover, New York
34. Chen JS, Han W, Wu CT, Duan W (1997) On the perturbed Lagrangian formulation for nearly incompressible and incompressible hyperelasticity. Comput Method Appl Mech Eng 142(3–4):335–351
35. Chen JS, Pan CH (1996) A pressure projection method for nearly incompressible rubber hyperelasticity.1. J Appl Mech Trans ASME 63(4):862–868
36. Chen JS, Wu CT, Pan CH (1996) A pressure projection method for nearly incompressible rubber hyperelasticity.2. Applications. J Appl Mech Trans ASME 63(4):869–876
37. Fried I (1974) Finite element analysis of incompressible material by residual energy balancing. Int J Solid Struct 10(9):993–1002
38. Zienkiewicz OC, Taylor RL, Too JM (1971) Reduced integration technique in general analysis of plates and shells. Int J Numer Method Eng 3(2):275–290
39. Malkus DS, Hughes TJR (1978) Mixed finite-element methods—reduced and selective integration techniques: a unification of concepts. Comput Methods Appl Mech Eng 15(1):63–81
40. Hughes TJR (1980) Generalization of selective integration procedures to anisotropic and nonlinear media. Int J Numer Method Eng 15(9):1413–1418
41. Belytschko T, Ong JSJ, Liu WK, Kennedy JM (1984) Hourglass control in linear and nonlinear problems. Comput Method Appl Mech Eng 43(3):251–276
42. Liu WK, Ong JSJ, Uras RA (1985) Finite-element stabilization matrices—a unification approach. Comput Method Appl Mech Eng 53(1):13–46
43. Vidal Y, Villon P, Huerta A (2003) Locking in the incompressible limit: pseudo-divergence-free element free Galerkin. Commun Numer Method Eng 19(9):725–735
44. Lovadina C, Auricchio F, da Veiga LB, Buffa A, Reali A, Sangalli G (2007) A fully "locking-free" isogeometric approach for plane linear elasticity problems: a stream function formulation. Comput Method Appl Mech Eng 197(1–4):160–172
45. Hughes TJR, Cottrell JA, Bazilevs Y (2005) Isogeometric analysis: CAD, finite elements, NURBS, exact geometry and mesh refinement. Comput Method Appl Mech Eng 194(39–41):4135–4195
46. Wu CT, Hu W, Chen JS (2012) A meshfree-enriched finite element method for compressible and near-incompressible elasticity. Int J Numer Method Eng 90(7):882–914
47. Franca LP, Stenberg R (1991) Error analysis of some Galerkin least-squares methods for the elasticity equations. SIAM J Numer Anal 28(6):1680–1697
48. Cai ZQ, Starke G (2004) Least-squares methods for linear elasticity. SIAM J Numer Anal 42(2):826–842

49. Micchelli CA (1986) Interpolation of scattered data—distance matrices and conditionally positive definite functions. Constr Approx 2(1):11–22
50. Madych WR, Nelson SA (1990) Multivariate interpolation and conditionally positive definite functions.2. Math Comput 54(189):211–230
51. Madych WR (1992) Miscellaneous error-bounds for multiquadric and related interpolators. Comput Math Appl 24(12):121–138
52. Ciarlet PG (1978) Mathematical elasticity vol I: three dimensional elasticity. North-Holland, Amsterdam
53. Timoshenko SP, Goodier JN (1934) Theory of elasticity. McGraw-Hill, New York
54. Chen JS, Pan C, Chang TYP (1995) On the control of pressure oscillation in bilinear-displacement constant-pressure element. Comput Method Appl Mech Eng 128(1–2):137–152
55. Zienkiewicz OC, Taylor RL, Zhu JZ (2005) The finite element method: its basis and fundamentals, 6th edn. Elsevier, New York